CHAPTER IV
ISOTROPICALLY SMALL CRYSTALLINE LAMELLAE INDUCED BY HIGH BIAXIAL-STRETCHING RATE AS A KEY MICROSTRUCTURE FOR SUPER-TOUGH POLYLACTIDE FILM

4.1 Abstract

At present, polylactide (PLA) film with high toughness is on expectation, but in general, it is brittle with 45 MPa tensile strength and only 3% elongation at break. The present work clarifies that isotropically small crystalline lamellae is the key microstructure to obtain super-tough PLA (180 MPa tensile strength and 80% elongation at break). The systematic study on two parameters of biaxial-stretching technique, *i.e.*, stretching rate and draw ratio, allows us understanding the development of microstructure, especially the crystalline phase, the regular chain packing in the crystal lattice, and the evolution of the higher-order structure. The integrated structural analyses based on Fourier transform infrared spectroscopy (FTIR), 2D-wide angle X-ray diffraction (2D-WAXD) and 2D-small angle X-ray scattering (2D-SAXS) declare that the structurally-irregular amorphous PLA starts to develop the mesophase and δ–crystal (including α–crystal) with the crystallite size of several tens of nanometers by slow biaxial-stretching (3 mm/s). At this stage, the biaxially oriented PLA (BOPLA) still shows relatively poor mechanical properties. When the stretching rate and the draw ratio increased above a certain level, *i.e.*, 75 mm/s and 5×5, respectively, the small δ–crystallites of about 10 nm size with isotropic orientation are mainly formed. This structural evolution has been found to result in the drastic increase of the toughness of BOPLA film, which is about 4 times higher than the PLA film produced by conventional stretching. In this way, the present work shows for the first time that the simple way to toughen the PLA film is to induce a well-dispersed higher-order structure consisting of many but small δ–crystallites as seen in the model case of BOPLA.

Keywords: polylactide, biaxial-stretching, microstructure

4.2 Introduction

PLA is accepted as the most potential biodegradable plastic for environmental concerns due to its reliable industrial-scale production. As PLA is a polyester, it can be processed variously as sheets, films, bottles, fibers and textiles. The main limitation of PLA is about its brittleness which mainly comes from the slow crystallization, especially when containing the isomer mixture [1-3]. In fact, when PLA is processed by various methods such as blown film extrusion, etc., the brittleness along the machine direction (MD) is significant. To overcome this point, several approaches to optimize the crystalline and amorphous phases, such as adding nucleating agents or plasticizers, controlling processing conditions, etc., were variously reported [4-11].

Biaxial-stretching (BO) is a processing technique which the polymer films can be oriented and as a consequence, the changes of microstructure give the drastic change in mechanical properties as well as other performances such as high-gloss, transparency, excellent gas barrier, etc [12-15]. These characteristics bring in the possible modern packaging for specific purposes, *e.g.*, cable insulation, metallizing lamination, industrial tapes, etc [13, 16]. In other words, we can expect the physicochemical properties improvements of polymers by simply changing their microstructures under the controlled BO process parameters, *i.e.*, stretching rate, draw ratio, temperature, and stretching mode (simultaneous or sequential).

The good example of the change in microstructure leading to the change in mechanical properties can be referred to the cases of biaxially oriented polyethylene (BOPE) [17, 18] and polypropylene (BOPP) [13, 14, 19-22]. For instance, Bobovitch *et al.* [17] studied biaxially oriented linear low density polyethylene (BOLLDPE) which was prepared by double bubble technique. This BOLLDPE showed the increased tensile strength but decreased tear resistance in MD when the MD draw ratio or *c*-axis orientation was increased. Lüpke *et al.* [19] reported the sequential BOPP with fixed MD draw ratio (λ_{MD} = 5) and varied transverse draw ratio (λ_{TD}). They found that the low λ_{TD} ($\lambda_{TD} \leq 2$) initiated the so-called shish kebab structure. This microstructure induced the increment of tensile strength and elongation at break by 3 and 2 times, respectively, when compared with the conventional PP film. In

contrast, they found that the high λ_{TD} ($\lambda_{TD} \geq 5$) provided the fibrillar network and at that time the stiffness in TD was significantly increased.

In the case of BOPLA, for example, Auras and coworkers [23] reported the lowering of CO_2 and O_2 permeability of BOPLA as compared to biaxially-oriented polystyrene and polyethylene terephthalate. These BOPLA films also showed relatively low water permeability coefficient with increasing of temperature which has potential in multilayer structures as claimed in many patents [24-28]. Up to the present, BOPLA is commercially available for food and non-food applications with various trade names such as NATIVIA™, Ecodear® Bio-Based films, BioPak®, etc.

It comes to the question that is how the BO process influences on the PLA microstructures. Ou and Cakmak [29] compared the microstructures of BOPLA films, produced *via* a stretching rate of 3 mm/s and draw ratios of 2×2 to 4×4 ($\lambda_{MD} \times \lambda_{TD}$) at 70 °C under varied stretching modes. The analyses by WAXD images and pole figures led to an understanding of the microstructure in terms of (i) in-plane isotropy of (200/110) diffractions with the degree of crystallinity (X_c) 15% and (ii) in-plane anisotropy with X_c 20% for simultaneous and sequential BOPLA, respectively. Additionally, they also extended the study to the annealed BOPLA films. This investigation presented the in-plane isotropy of (100) planes parallel to the surface for annealed simultaneous BOPLA whereas the uniplanar axial (100)[001] texture with mainly oriented in TD was found for annealed equally-sequential BOPLA [30]. Smith *et al.* [31] clarified that the decreased shrinkage of 4×4-BOPLA film was caused by low D-isomer content and the strain-induced crystalline network with anisotropic orientation, but independent on amorphous phase relaxation. Tsai and coworkers [32] reported that once the 3×3-BOPLA was stretched at 75 °C with the rate of 25 mm/s, the structure of the film became stable enough to reduce the shrinkage by 20% above the cold crystallization temperature. Delpouve *et al.* [33] clarified that the BOPLA formed the homogeneous orientation of the crystallites in the film plane (or orthotropic structure), allowing the decrease of water permeability by 40%.

As mentioned above, most studies on BOPLA are about a particular specific stretching condition and the properties obtained. The study of BOPLA under the systematic variation of the processing parameters, especially the stretching rate and

the draw ratio, to clarify the steps of the change in microstructure has not yet been reported. In fact, we carried out a preliminary experiment by varying the stretching rate and draw ratio of BOPLA at 90 °C in order to observe their mechanical properties. We found that when the stretching rate was as high as 75 mm/s with 5×5 draw ratio, it is for the first time that the BOPLA film reached a high toughness with 4-fold increase of tensile strength and 10-fold extension of elongation at break as compared with those of the conventional PLA blown films and the BOPLA obtained from the lower stretching rates (Figure 4.1). This suggests the specific microstructure of PLA developed as a consequence of the high biaxial-stretching rate and the high draw ratio.

The present work, therefore, focuses for the first time on the clarification for how the PLA microstructures are developed by BO process under the systematic variation of processing conditions. The work also shows the integrated information of microstructural analyses by FTIR spectra, thermal analysis, and X-ray structural analyses (2D-WAXD, and 2D-SAXS) and establishes the relationship between the microstructure and mechanical properties. In other words, an understanding of PLA microstructure and its consequent mechanical properties enable us to obtain an as-desired PLA mechanical properties by simply controlling the processing conditions.

4.3 Experimental

4.3.1 BOPLA Films Preparation

PLA resin (Ingeo™ grade 4043D) with the L-lactide content of 94% was from NatureWorks LLC, USA. The weight-average and number-average molecular weights were 166 kDa and 116 kDa, respectively, with polydispersity index of 1.43 as determined by gel permeation chromatography. The resin was processed by a Labtech Engineering chill roll casting film extruder in the temperature range of 155 - 175 °C to form PLA precursor sheet and it was used for BO process in the next step. The PLA precursor sheet obtained was cut into specimens (96×96×0.5 mm^3) and preheated at 90 °C for 30 s before simultaneous biaxial-stretching at the stretching rate of 3, 16, 37 and 75 mm/s or the strain rate of 4, 22, 50 and 100% s^{-1}, respectively, by using a Brückner KARO IV laboratory

biaxial stretcher. The draw ratios were 3×3 and 5×5 to obtain a series of BOPLA films. All the BOPLA films were quenched to room temperature (25 °C).

4.3.2 Characterization

Young's modulus, tensile strength and elongation at break of the films (1 × 10 cm^2) were measured by a Lloyd LRX tensile testing machine with a cross head speed of 50 mm/min and a tensile load of 0.5 kN at 25 °C according to ASTM D-638. The analysis along MD was repeated 10 times for each sample at the center area.

The ATR (attenuated total reflection) infrared spectra were obtained by using a Thermo Scientific Nicolet 6700 Fourier transform infrared (FTIR) spectrometer with a resolution of 2 cm^{-1} and triplicate measurements at the center area in different samples.

Thermal analysis was performed by using a Netzsch 200 F3 Maia differential scanning calorimeter (DSC). The samples were heated from 30 °C to 200 °C at a heating rate of 5 °C/min under nitrogen gas at a flow rate of 50 mL/min. The X_c was calculated by using Eq. 1:

$$X_c = \frac{(\Delta H_{m,PLA} - \Delta H_{c,PLA}) \times 100}{\Delta H^0_{m,PLA}} \quad \text{(Eq. 1)}$$

where $\Delta H_{m,PLA}$ and $\Delta H_{c,PLA}$ were the enthalpy changes of fusion at ~150 °C and cold crystallization in the temperature range of 70 - 120 °C, respectively. The $\Delta H^0_{m,PLA}$ is 93 J/g for 100% crystalline PLA as reported by Fischer *et al.* [34]. The temperature dependence X-ray diffraction measurement was also carried out by using a Rigaku TTR-III X-ray diffractometer with Cu-Kα line as an incident X-ray beam. The temperature range was 0 °C to 170 °C at a heating rate of 2 °C/min. Assuming that the crystalline lattice is free of defect, the crystallite size <L> was evaluated on the basis of Scherrer's equation (Eq. 2) [35].

$$\langle L \rangle = \frac{K\lambda}{\beta_{1/2}\cos\theta} \quad \text{(Eq. 2)}$$

where $\beta_{1/2}$ is the full width at half maximum, λ is the wavelength of Cu-Kα radiation (1.5418 Å), and K is the broadening constant of 0.9 for the imperfect polycrystal [36].

The two-dimensional wide angle X-ray diffraction (2D-WAXD) and small angle X-ray scattering (2D-SAXS) patterns of the stacked samples of 0.5 - 1 mm thickness were taken by using a Rigaku R-axis VII X-ray diffractometer and a Rigaku Nano-viewer, respectively. Mo-Kα line as an incident X-ray beam and a flat imaging plate detector with 110 mm sample-to-camera distance were used for the 2D-WAXD pattern measurement. For the 2D-SAXS pattern measurement, the Cu-Kα line and a Dectris Pilatus detector with 120 cm sample-to-camera distance were applied. The scattering angle (2θ) was converted to scattering vector (q) defined as $q = (4\pi/\lambda)\sin(\theta)$. The thermal investigations and the 2D-WAXD and 2D-SAXS measurements were carried out along MD at the center area of the PLA precursor sheet and BOPLA films in triplicate.

4.4 Results and Discussion

4.4.1 Mechanical Properties of BOPLA Films

During the BO process, the change in apparent stress of PLA precursor sheet was traced. The sheet showed a strain-hardening, which corresponds to the cohesiveness of the crystalline phase of PLA induced by the BO process. The BOPLA by 5×5 draw ratio can be successfully obtained when the stretching temperature was higher than 90 °C. This was also reported by Chapleau *et al.* [4].

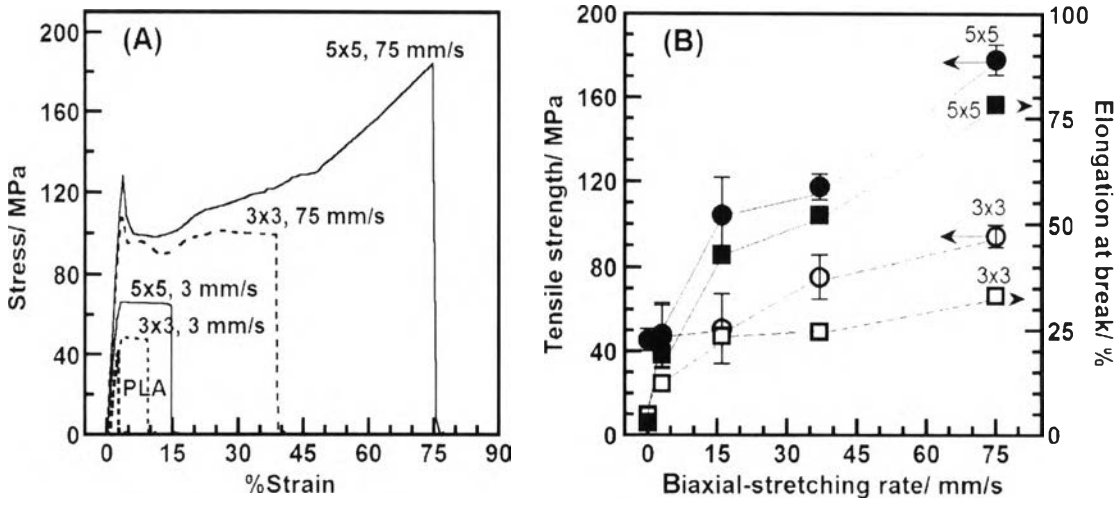

Figure 4.1 (A) Stress vs strain curves and (B) plots of mechanical properties as a function of biaxial-stretching rate of PLA and BOPLA films.

In general, a commercial PLA blown film is rigid and brittle with Young's modulus ~2.2 GPa, tensile strength ~45 MPa, and 3-5% elongation at break (as presented in Figure 4.1). In order to follow how the BO process changes the mechanical properties of PLA films, the stretching rate and the draw ratio were varied. Figure 4.1A and Figure 4.1B show the stress-strain curves and the mechanical properties of BOPLA films, respectively, after the PLA precursor sheet was biaxially-stretched at different stretching rates and draw ratios. When the stretching rate was as high as 75 mm/s, the stress-strain curve changes drastically from brittle PLA blown film (PLA) to ductile films (3×3 and 5×5, 75 mm/s). As seen in Fig. 1B, the tensile strength and elongation at break are increased remarkably by increasing of stretching rate and draw ratio. In particular, the tensile strength and the elongation at break of BOPLA prepared by 5×5 draw ratio at 75 mm/s stretching rate are almost 4 and 20 times higher than those of the PLA blown film, respectively.

4.4.2 Crystallization and Crystal Phase of BOPLA Films

4.4.2.1 Observing Crystalline Phase and Mesophase

Basically, the microstructure regularization of PLA presents the α– and β–forms of crystals when PLA was produced by general processes [37]. The incomplete crystal of α–form, namely, α'– or δ–form and mesophase

(intermediate phase to be developed to δ– and α–forms, subsequently) are also found when the stretching is applied at near glass transition temperature (T_g ~ 60 °C) of PLA [38-42].

Herein, ATR-FTIR technique was preliminary applied to characterize the developed regularization of BOPLA microstructure. The important characteristic IR peaks of the α– and/or δ–phase, amorphous phase, and mesophase of PLA are identified at 921, 958, and 1268 cm^{-1}, respectively, which are similar to the reports by Stoclet *et al.* [40], Wasanasuk and Tashiro [42] and Na *et al.* [43]. Fig. 2 shows the amorphous phase peak at 958 cm^{-1}, which appears in all 3×3- and 5×5-BOPLA films. The band at 921 cm^{-1} or the crystalline band is detected for the first time when the stretching rate was above 16 mm/s. This suggests that the crystalline phase of PLA is induced obviously as a consequence of BO process with relatively fast stretching.

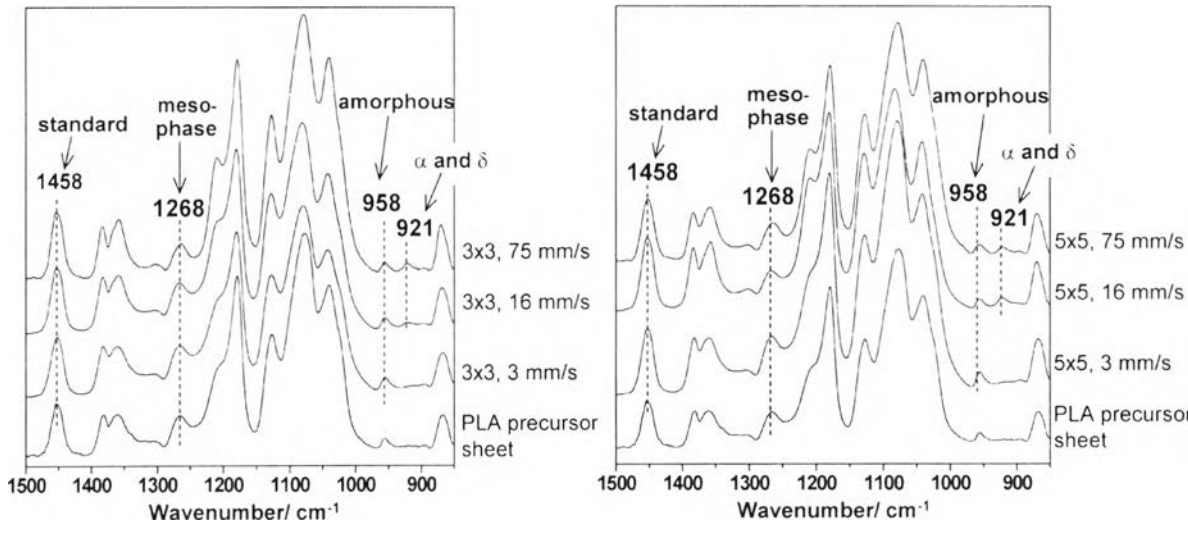

Figure 4.2 ATR-FTIR spectra of PLA precursor sheet, and 3×3- and 5×5-BOPLA films with varied biaxial-stretching rate.

In order to quantitatively evaluate the increases of the crystalline phase and mesophase when the processing conditions were changed, the curve fitting analyses of the peaks at 921 and 1268 cm^{-1} were carried out. The peak at 1458 cm^{-1} (CH_3 deformation) was used as the internal standard so that it is possible

to compare the IR intensity of varied BOPLA films even their thicknesses were different. The intensity ratios of I_{921}/I_{1458} and I_{1268}/I_{1458} represent the relative contents of the α– and/or δ–phase, and mesophase, respectively.

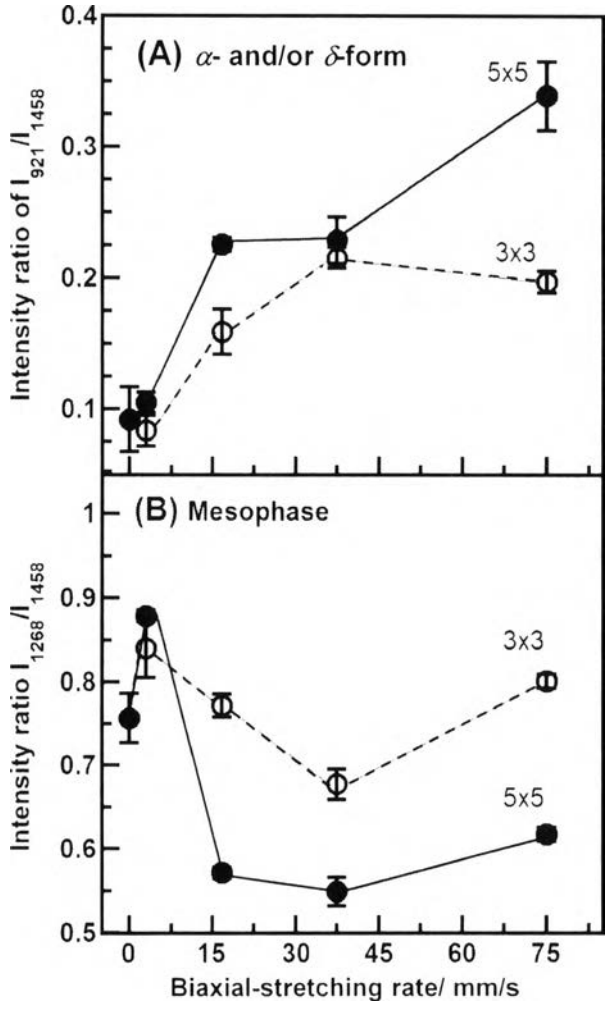

Figure 4.3 ATR-FTIR peak intensity ratios of crystalline phase and mesophase of various BOPLA films as a function of biaxial-stretching rate.

Figure 4.3 shows the dependence of the relative contents of these phases on the stretching rate at 3×3 and 5×5 draw ratios. In the case of 3×3-BOPLA, the relative content of the α– and/or δ–phase increases when the stretching rate was higher than 16 mm/s. The increase is much more significant when the 75

mm/s stretching rate was combined with 5×5 draw ratio. In other words, this condition causes a significant increase of α– and/or δ–phase.

For the mesophase, its content increases by the low stretching rate of 3 mm/s, and then decreases by moderate stretching rates (16 and 37 mm/s). A small increase is detected at the high stretching rate (75 mm/s) for both 3×3- and 5×5-BOPLA. The appearances of the mesophase and the α– and/or δ–phase by high stretching rate imply that the unoriented PLA chains in amorphous region rearrange themselves to the ordered structures.

4.4.2.2 WAXD Patterns and Crystallite Size of BOPLA Films

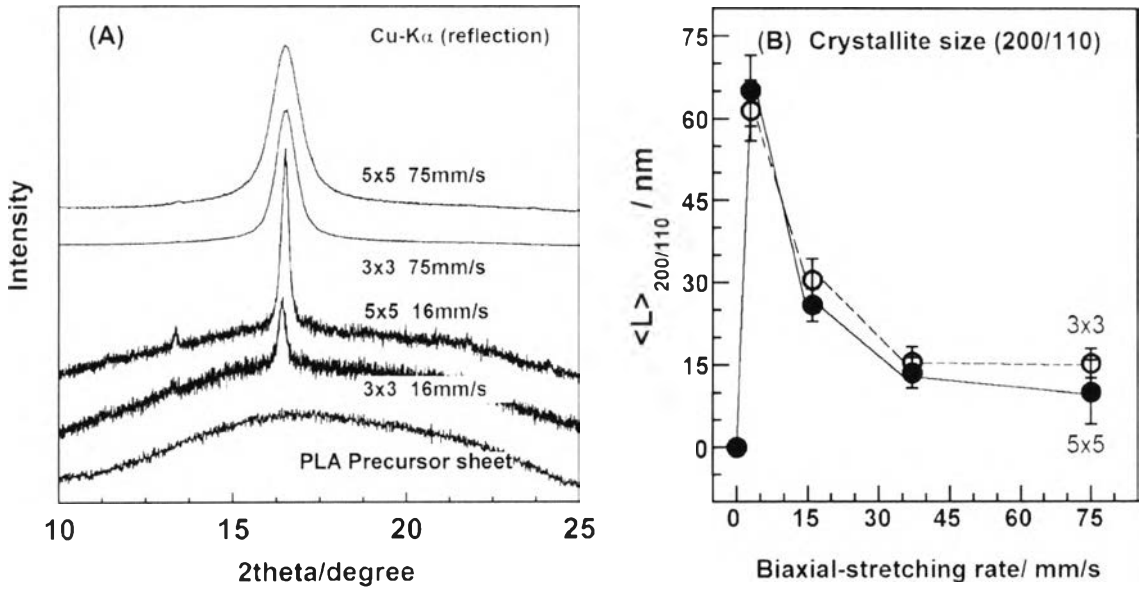

Figure 4.4 (A) WAXD patterns at room temperature (25 °C) and (B) crystallite size $<L>_{200/110}$ of 3×3-, and 5×5-BOPLA.

In order to clarify the details of the chains regularization obtained from the BO process under the varied stretching rates and draw ratios, the temperature dependence X-ray diffraction (WAXD) measurement was performed. Figure 4.4A shows the WAXD patterns obtained at room temperature (25 °C) for the PLA precursor sheet and the BOPLA films with different stretching rates and draw ratios. The PLA precursor sheet shows a broad diffraction pattern as assigned to

amorphous phase, similar to that of the PLA blown film. When the stretching rate was 16 mm/s, the broad amorphous phase with a sharp (200/110) peak of crystalline phase at 16.3° 2θ is observed. When the draw ratio was increased to 5×5, the amorphous phase gradually decreases and the 16.3° 2θ peak became significant. When the stretching rate was as high as 75 mm/s, BOPLA shows a single broad peak at 16.5° 2θ assigned to the δ–phase and the amorphous phase is almost negligible. It should be noted that if the film contains the perfect α–phase, the strong diffraction peaks at 12.4°, 14.7°, 19.1°, 22.1°, and 23.5° 2θ, should be presented.

In this way, the BOPLA, stretched at the high stretching rate, induces a transition to the ordered phase effectively (Figure 4.4A). It is important to note that the crystalline peak is much broader, compared to the case of the lower stretching rate (16 mm/s). The crystallite size (<L>) was estimated from the half width of the reflection peak by using the Scherrer's equation. Figure 4.4B shows the thus-estimated crystallite size obtained along (200/110) diffraction ($<L>_{200,110}$) as a function of biaxial-stretching rate. In the case of 3×3-BOPLA, the 3 mm/s stretching rate gives the relatively large crystallite size $<L>_{200,110}$ of about 60 nm (Figure 4.4B). Whereas the stretching rate was increased to 16, 37, and 75 mm/s, it effectively brings the decrease of $<L>_{200,110}$ to 30, 16, and 15 nm, respectively. The 5×5 draw ratio shows the similar behavior. This confirms that the fast stretching leads to the growth of the relatively small δ–crystallites.

4.4.2.3 Higher-order Structure Change in BOPLA Films

To investigate the higher-order structure change caused by the BO process, the 2D-WAXD and 2D-SAXS analyses were performed. Figure 4.5 and Figure 4.6 show the 2D-SAXS and 2D-WAXD patterns of the PLA precursor sheet and BOPLA films produced by the draw ratios of 3×3, and 5×5, respectively.

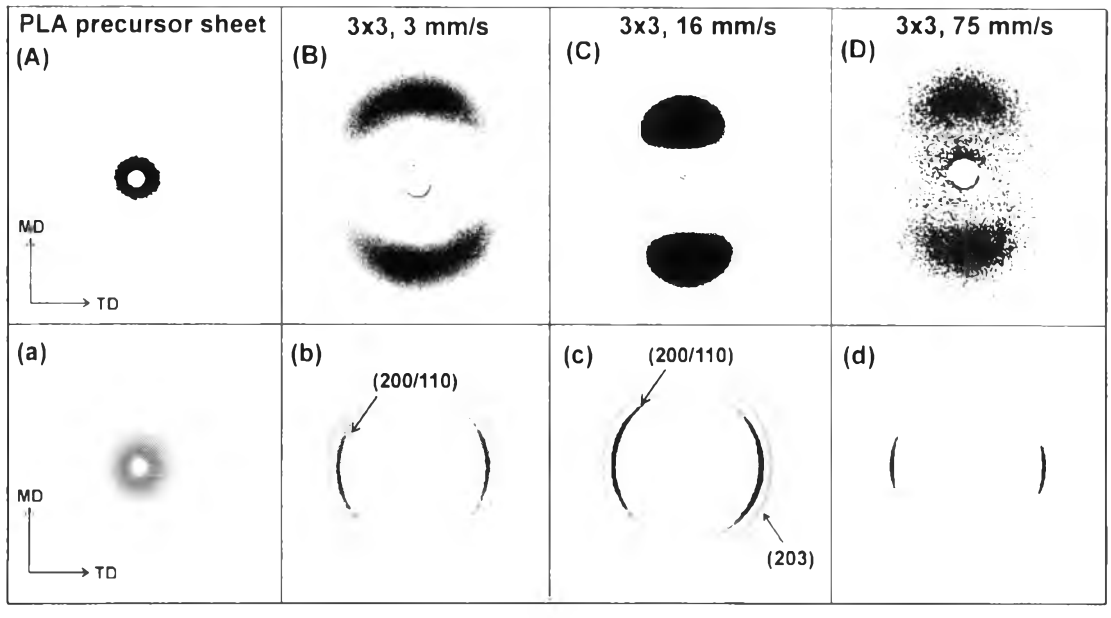

Figure 4.5 2D-SAXS (upper) and 2D-WAXD (bottom) patterns of PLA precursor sheet and 3×3-BOPLA films obtained from biaxial-stretching rates of 3, 16, and 75 mm/s, respectively.

In the case of Figure 4.5A, the profile observed is confirmed to be the pattern obtained from the beam stopper. This means that there is no any scattering pattern observed from PLA precursor sheet. At the same time, the WAXD pattern of this PLA precursor sheet also shows the amorphous halo in Figure 4.5a, as similar to the study of Delpouve *et al.* [44]. In fact, our PLA precursor sheet shows the IR peak at 1268 cm^{-1} (Figure 4.2) whereas Stoclet *et al.* reported the WAXD pattern at 16° implying the mesophase of PLA [45]. Here, when Figure 4.5a was integrated to intensity profile, the similar broad peak at 16° referred to the mesophase was also observed (Supporting information S1). The BO process causes a certain degree of orientation (Figure 4.5B-D). In the case of 3×3-BOPLA obtained at 3 mm/s stretching rate (Figure 4.5B), the 2D-SAXS pattern shows an arcade pattern, indicating that the stacked lamellae were oriented more or less along MD but the degree of orientation was not very high. This stacked lamellar orientation increases for the sample at the higher stretching rate (16 mm/s) as seen from the observation of meridional scattering spots in Figure 4.5C. The BOPLA prepared at 75 mm/s (Figure 4.5D, d) shows the relatively high orientation along the meridional direction in both

2D-WAXD and 2D-SAXS patterns. It must be noted here that the lamellae were oriented preferentially along MD, although the sample was stretched simultaneously along MD and TD in the case of 3×3 draw ratio. This suggests that the PLA precursor sheet was originally oriented preferentially along MD during casting as seen from the broad peaks at 85° and 260° when the PLA precursor sheet was azimuthally scanned (Supporting information S2). Such relatively low draw ratio as 3×3 cannot erase this preferential orientation well enough to give the isotropic orientation attained in the ideal case.

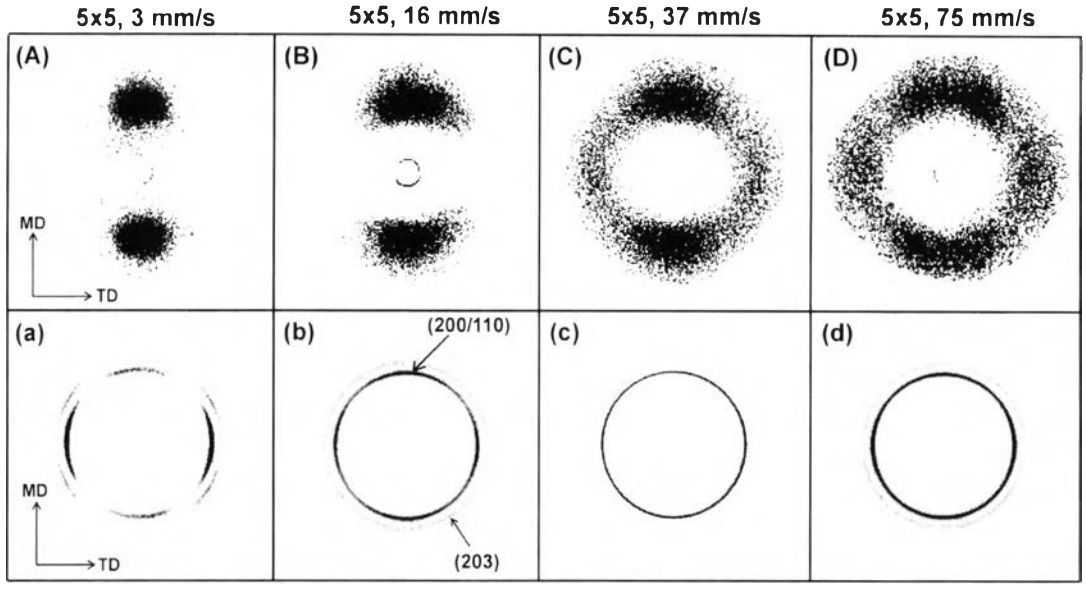

Figure 4.6 2D-SAXS (upper) and 2D-WAXD (bottom) patterns of 5×5-BOPLA films produced under various stretching rates.

The effect of BO process can be seen more clearly in the case of 5×5-BOPLA (Figure 4.6). The low stretching rates (Figure 4.6A-B) still give the preferential orientation of lamellae along MD. The 2D-WAXD pattern also gives the preferential MD orientation of crystalline lattices, consistent with the 2D-SAXS data. The stretching rates of 37, and 75 mm/s give the 2D-SAXS pattern different from the others (Figure 4.6C-D). The scattering peaks can be detected in the meridional and equatorial directions. The scattering pattern developed in TD is more intense by increasing of stretching rate as evidenced from the intensity of scattering for the 75 mm/s stretching rate, higher than that for 37 mm/s. It should be noted that the

lamellae, which were originally oriented preferentially along the MD, are now reoriented toward the TD also by applying the fast stretching and the high draw ratio. Correspondingly, as seen in the 2D-WAXD pattern of Figure 4.6C-D, the ring patterns of (200/110) and (203) reflections are detected to show relatively homogeneous orientation of the crystal lattices.

Considering the degree of orientation (f), it should be noted that the f value can be shifted when the ordered packing structure changed, and consequentially, influenced on BOPLA properties as demonstrated by Tsuji *et al.* [46]. Here, the f values were also calculated from azimuthal angle (φ) scan. For f=1 at 0° and 90° (φ), they were assigned to polymer chains aligned parallel and perpendicular to MD, respectively. When the isotropic orientation was formed as observed from 5×5-BOPLA by high stretching rate (Figure 5.6C-D), the f values at 0° and 90° (φ) of (200/110) and (203) diffraction planes decreased significantly and became close to zero (Supporting information S3). In other words, there was no any orientation in a specific direction (*i.e.* MD or TD) when the isotropy in-plane was occurred.

The structural parameters were determined by using the 2D-SAXS patterns, as shown in Figure 4.5 and Figure 4.6. The results are shown in Figure 4.7a-c where the long period, size, and thickness of the stacked lamellae are plotted against the biaxial-stretching rate for 3×3 and 5×5–BOPLA, respectively, (see calculation in Supporting information S4). In the case of 3×3-BOPLA, the long period was almost constant with an increase of stretching rate (Figure 4.7A,a). This implied that the 3×3 draw ratio is not effective enough to bring in the significant change in the long period. The size of stacked lamellae decreases (Figure 4.7A,b), while the lamellar thickness increases at the relatively low stretching rate but it gradually decreases with an increment of stretching rate (Figure 4.7A,c). On the other hand, in the case of 5×5-BOPLA (Figure 4.7B), the long period decreases remarkably with the decreased stacked lamellar size as the stretching rate was increased. In this way, for the high draw ratio, the increment of stretching rate effectively produces the stacked structure of lamellae with relatively small size. This is consistent with the results of Figure 4.4B. At the same time, as seen in the DSC

result (Figure 4.9), the X_c is found to increase with an increase of stretching rate (more discussion in *Thermal behaviors of BOPLA films*).

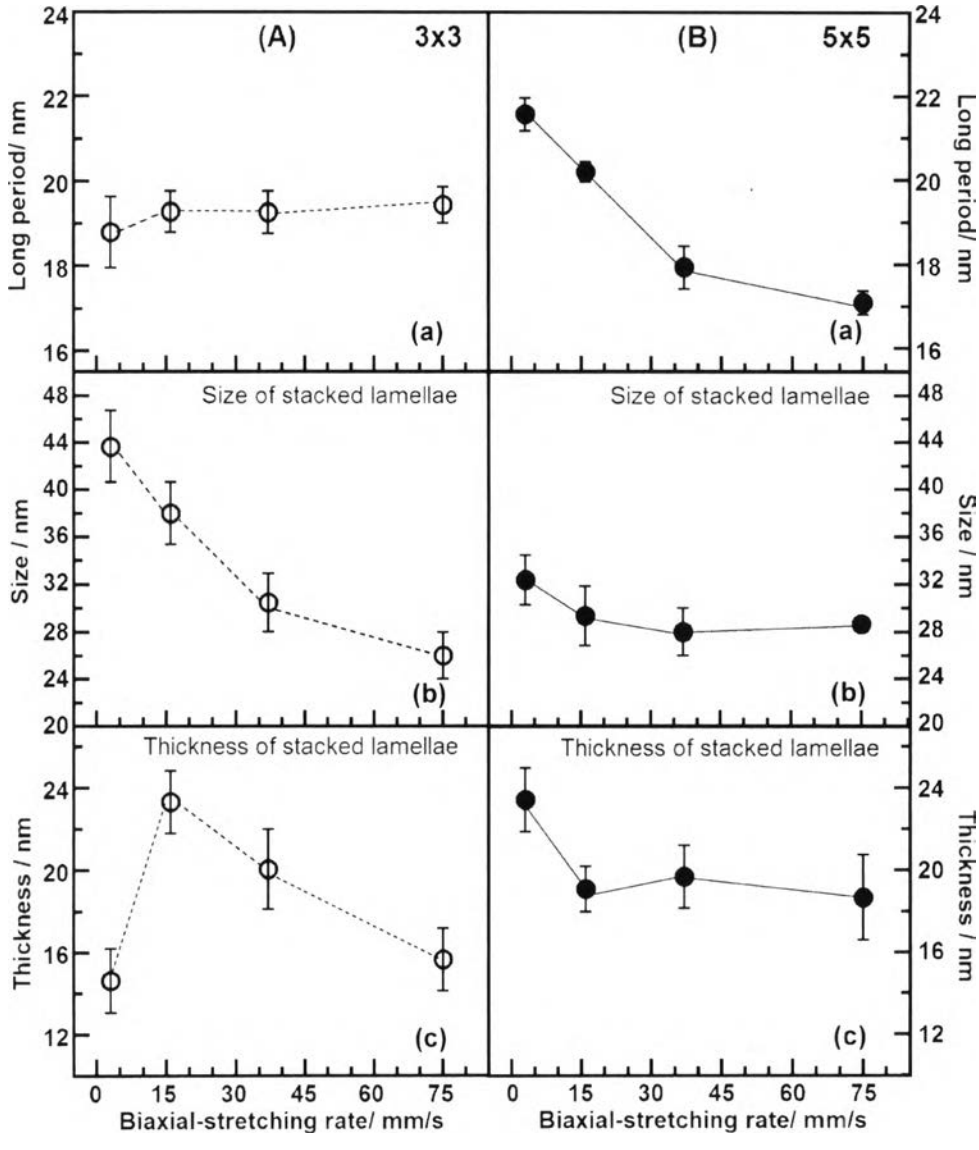

Figure 4.7 Long period, size and thickness of stacked lamellae as a function of stretching rate for (A) 3×3-, and (B) 5×5-BOPLA films.

Figure 4.7 leads to the information of the microstructure as follows. The combination of slow stretching and relatively low draw ratio gives the small amount of the appreciably large stacked lamellae with the high degree of orientation parallel to MD. In contrast, the fast stretching with the high draw ratio produces the large amount but relatively small lamellae which are gathered together

under the highly isotropic orientation and X_c. These two largely different microstructures or morphologies may play an important role in the remarkable change in the mechanical properties shown in Figure 4.1. As also found in annealed PLA by the study of Tsuji and Ikada [47], the high amount of small PLA crystallites provided the increases of tensile strength and Young's modulus.

4.4.2.4 Thermal Behaviors of BOPLA Films

As discussed above, the BO process leads to the remarkable changes in the microstructure of PLA. These morphological changes should also reflect directly on the thermal behavior in the heating process up to the melting point. The simultaneous measurement of WAXD and DSC thermogram was performed to clarify this point.

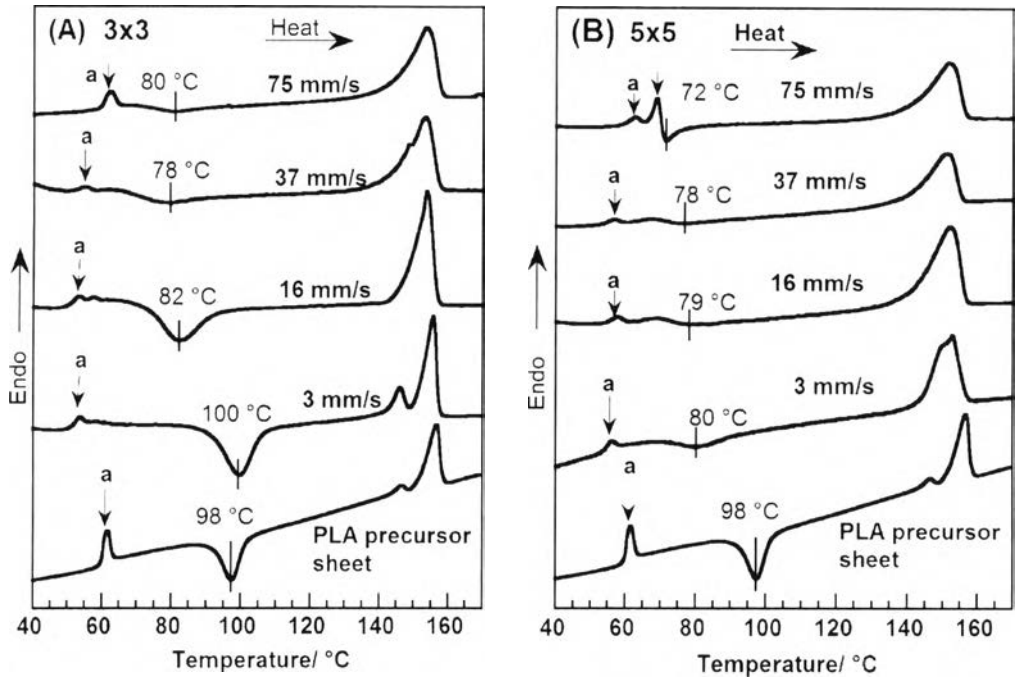

Figure 4.8 DSC thermograms of BOPLA films at draw ratios of (A) 3×3 and (B) 5×5 by varied stretching rates.

Figure 4.8 shows DSC thermograms of PLA precursor sheet and all BOPLA films with the remained T_g at ~60 °C. A small endothermic peak (arrow a), as clearly observed in PLA precursor sheet, is detected just above T_g

referring to the enthalpy relaxation in amorphous phase. It corresponds to the reorganization of mesophase, produced in the BO process, to form the higher-order structure (*i.e.* δ– and/or α–form) at higher temperature, as already clarified by Wasanasuk and Tashiro [42]. A broad exothermic peak was detected at around 98 °C for the precursor sheet, corresponding to the recrystallization to the δ–form. This transition temperature of 3×3-BOPLA is found to shift toward the lower temperature side as the stretching rate was increased. A shoulder or a small peak below the melting peak corresponds to the δ to α transition. Figure 4.8B obtained for 5×5-BOPLA also shows the similar behaviors with the remarkable shift of the exothermic peak. The details of the structural changes occurring at the individual endo- and exothermic peaks are revealed by performing the simultaneous measurement of WAXD and DSC (see discussion in Figures 4.10, 4.11 and 4.12).

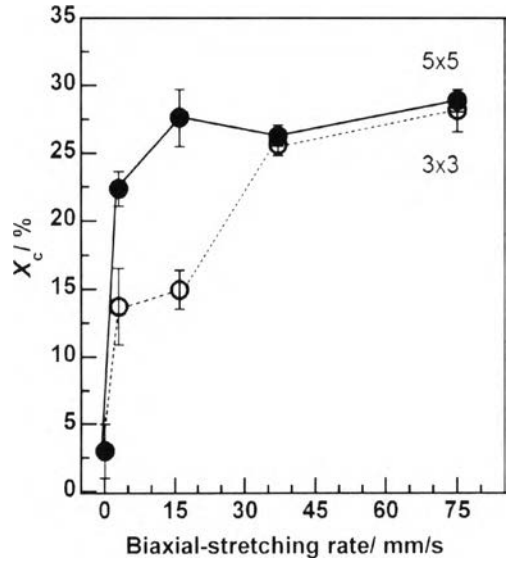

Figure 4.9 Plots of X_c derived from DSC thermograms against the stretching rate for 3×3- and 5×5-BOPLA films.

The X_c was estimated from the endothermic peak area at the melting point. The result is shown in Figure 4.9. The X_c of PLA increased remarkably by biaxial-stretching. The X_c increases dramatically when the sample was stretched by 3×3 and 5×5 at slow rate of 3 mm/s. The X_c of 3×3-BOPLA increases

furthermore when the sample was stretched at a higher rate. By the fast stretching, *i.e.*, 37 and 75 mm/s, the X_c is remained at ~30%, although the draw ratio was increased.

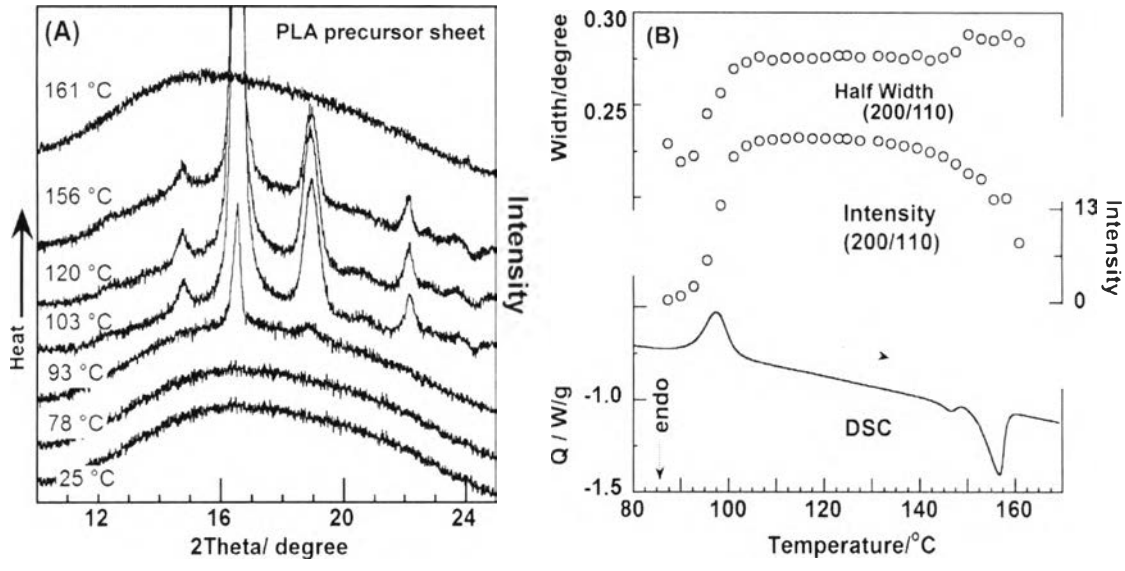

Figure 4.10 (A) Temperature dependence of WAXD patterns, and (B) DSC thermograms with intensity and half width of (200/110) diffraction for PLA precursor sheet.

Figure 4.10A shows the temperature dependence of WAXD profile measured for the PLA precursor sheet. As already pointed out, the sample was almost amorphous at room temperature. Even when the sample was heated above T_g, the sample was still in the amorphous phase as evidenced from no change in WAXD profile. When the temperature was increased to about 90 °C, a sharp but single diffraction peak of the δ-form developed from mesophase appears, where an exothermic peak is detected in the DSC thermogram. In a wide temperature region of 100 °C – 130 °C, the δ-form is detected as observed from the presence of the strong diffraction peaks at 14.7°, 16.5°, 19.1° and 22.1° 2θ. Just below the melting point at 155 °C, a small peak is observed as an endothermic peak of the DSC with decreasing of (200/110) diffraction intensity (Figure 10B), where the δ-form transition to the α-form occurred.

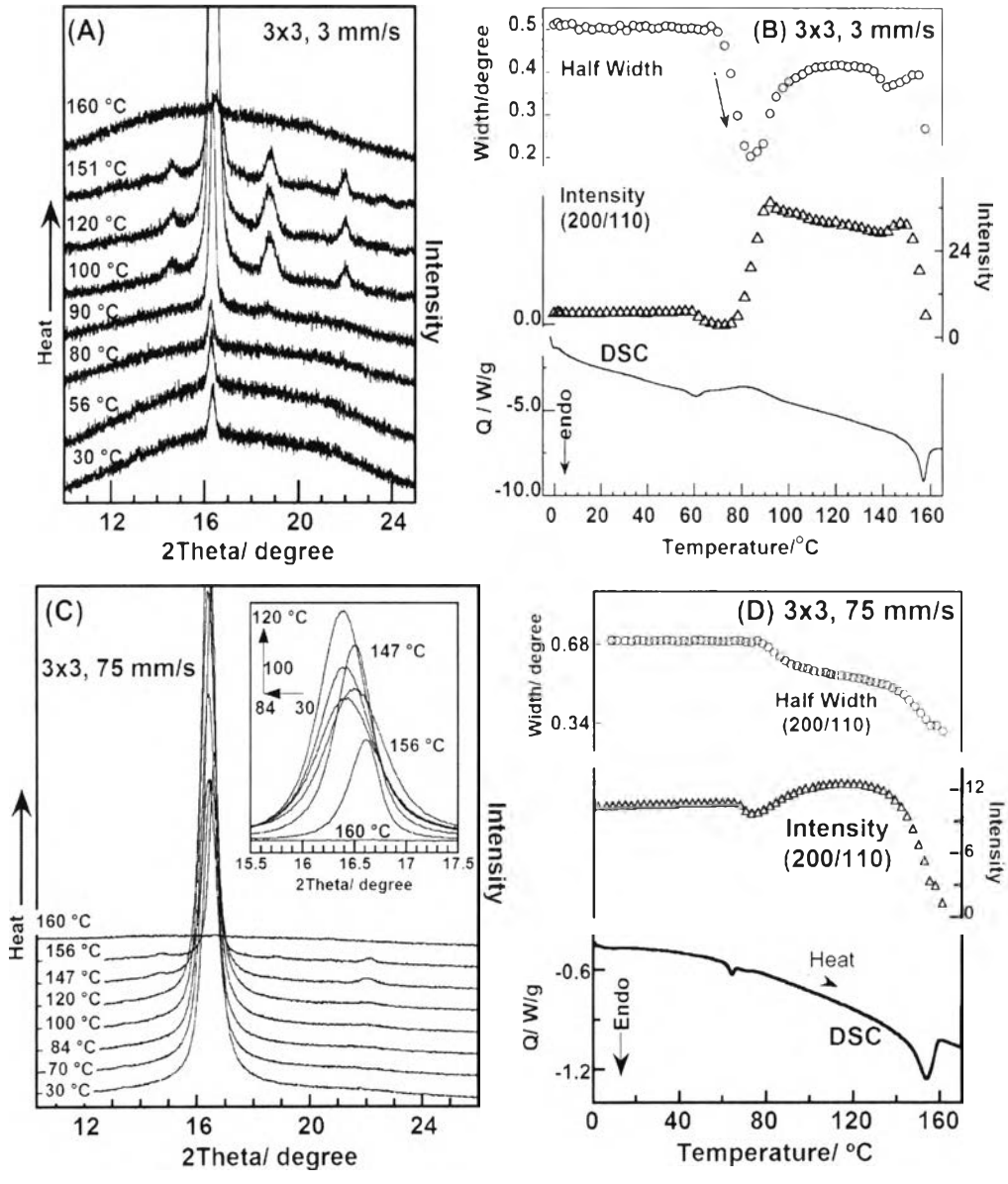

Figure 4.11 Temperature dependence of WAXD patterns, and intensity and half width of (200/110) diffraction compared with DSC thermograms measured simultaneously for 3×3-BOPLA by (A, B) 3, and (C, D) 75 mm/s, respectively.

In the case of 3×3-BOPLA at 3 mm/s, the starting sample contained the small amount of δ–phase, as seen in a sharp but isolated peak at around 16.5° 2θ, and mesophase which further developed to the δ–form and then to the α–form in a higher temperature region (Figure 4.11A) as evidenced from the significant

decrease of half width and increased intensity of (200/110) diffraction at above 60 °C (Figure 4.11B). The 3×3-BOPLA stretched at a high rate of 75 mm/s shows the peak of the δ-form at the starting point of heating process or room temperature (Figure 4.11C). In the exothermic peak region at around 75 °C, the δ-form peak decreased in intensity once and then increased gradually in the higher temperature region (Figure 4.11D). This may be due to the enthalpy relaxation of the originally contained mesophase, and consequently, the mesophase recrystallization into δ-form. The sharpening of the diffraction peak is consistent with this structural regularization. Notably, when the temperature was higher than 120 °C, this (200/110) peak shifts backward to the higher 2θ with slightly sharp peak and decrease in its intensity. This implies the δ to α phase transition. The small endothermic peak followed by a broad exothermic peak of the DSC can be always detected for the 3×3-BOPLA prepared at the different stretching rates (Figures 4.8A, 4.11B, and 4.11D). This endothermic peak region shifted toward the lower temperature side, it points out the mesophase transition to the δ-form preferentially occurred at the higher stretching rate.

The similar observation was also made for the 5×5-BOPLA. As seen already in the DSC thermograms shown in Figure 4.8, the small endothermic peak followed by a broad exothermic peak can be observed in this sample. The peak position is almost the same irrespective of the stretching rate. As shown in Figure 4.12, the simultaneous measurement of WAXD and DSC revealed the structural change along these thermal energy changes: the enthalpy relaxation of the mesophase (at around 70 °C) followed by the appearance of the δ-form (at around 80 °C) is detected in the X-ray diffraction measurement, which corresponds well to the temperature regions of the thermal energy changes.

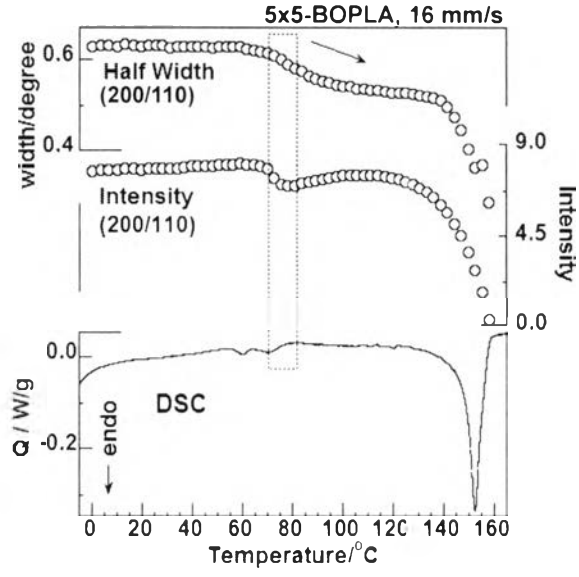

Figure 4.12 Intensity and half-width of (200/110) diffraction compared with the DSC thermogram measured simultaneously for 5×5-BOPLA at 16 mm/s stretching rate.

In summary, the PLA precursor sheet exists in an amorphous phase mainly, which transforms to mesophase followed by the regularization to the δ– (and α–) form in a higher temperature region. The 3×3-BOPLA exists in mesophase with the small amount of δ–phase. By heating, the mesophase rearranges once, and then, recrystallizes to the δ–form in an exothermic region. As the stretching rate is increased, the regularization of mesophase to δ–form occurs in a lower temperature region. More highly stretched BOPLA (5×5) shows sharper transition to δ–form at the exothermic peak around 72 °C. As seen in the WAXD profile detected at room temperature (Figure 4.4A) and the 2D-WAXD pattern (Figure 4.6), the 5×5-BOPLA prepared at a higher stretching rate, *i.e.*, 75 mm/s, contains much higher amount of the δ–form in addition to the mesophase, although their size is about 4 times smaller compared with that of the sample prepared at lower stretching rate.

4.4.3 Integrating Microstructure Information with the Mechanical Properties

The detailed analyses of the microstructure developed in BOPLA films lead us to the understanding of the drastic changes of BOPLA mechanical properties shown in Figure 4.1. Scheme 4.1 illustrates the microstructure change speculated for each BOPLA. The PLA precursor sheet is in an amorphous state with some mesophase. When it was biaxially-stretched, the crystalline phase was gradually developed depending on the stretching rate. For the stretching condition at 3 mm/s, BOPLA showed the coexistence of the mesophase and δ-phase with the crystallite size of about 60 nm and the X_c of about 15% - 25%. The crystallite size decreased to a half when the stretching rate was increased to the moderate rate (16 mm/s) whereas the lamellae mainly aligned anisotropy in-plane in preferential MD. This brought a slight improvement on mechanical properties of PLA as seen from the increase in tensile strength and elongation at break for 2 and 10 times, respectively. When the stretching rate was further increased, the lamellar size was decreased significantly. When the draw ratio was increased to 5×5 combined with 75 mm/s, the δ-phase became the main crystal form with the reduced $<L>_{200,110}$ to 10 nm. The X_c reached the maximum at 30%. At this BO condition (5×5, 75 mm/s), the BOPLA showed a certain level of isotropic orientation. The careful analyses let us know that this orientation was composed of the smallest crystalline lamellae with the closest stacking (or the decrease of the long period) as compared to other stretching rates and draw ratio. In fact, this high-order structure of BOPLA gives the remarkable mechanical properties with high tensile strength (more than 4 times) and elongation at break (more than 20 times). It is also important to note that the results in Figures 4.10, 4.11 and 4.12 are the integrated information of the changes in temperature and the packing structure of BOPLA. All changes of 5×5-BOPLA developed in Figure 4.12 in terms of sharpen half width of (200/110) planes, and slightly decreased (200/110) diffraction intensity, therefore, were started from the original packing structure (δ-form) of Scheme 4.1(C).

Scheme 4.1 Illustration for microstructure change of BOPLA films under varied biaxial-stretching rates.

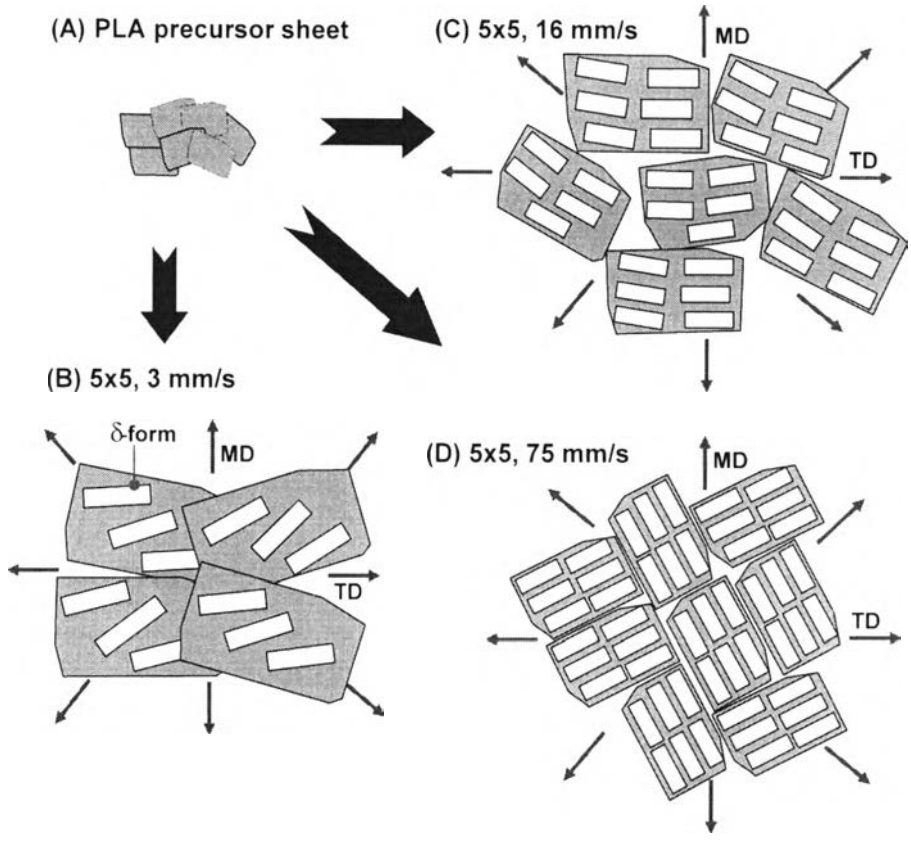

4.5 Conclusions

The conventional PLA film is comparatively brittle and becomes a main problem. In this study, the simultaneous BO process has been applied to the PLA film. In the past, there were several reports about BOPLA films [23-33], but the present work is totally different from theirs in such a point that the quite high stretching rate was applied for the first time. It gave the film with remarkably enhanced mechanical properties. The detailed analyses of WAXD, SAXS, FTIR spectra and DSC thermograms have revealed the existence of characteristic morphology in such a speedily-stretched BOPLA film. That is to say, the presence of many small but highly-oriented crystallites is considered to give the remarkable enhancement of tensile strength and elongation at break. As well known, the existence of many small grains is important for the production of steel with excellent mechanical toughness [48]: the smaller the grains size results in the harder toughness

of steel. The similar situation was detected for the BOPLA films: the crystallite size and the toughness are, roughly speaking, in the inverse relation with each other as seen from the comparison among Figures 4.1B, 4.4B, and 4.7. In fact, as shown in Figure 13, a good linear relationship between the mechanical properties and the inversed crystallite size for the BOPLA films prepared at the different conditions is successfully established. Of course, steel and polymer might have the different morphology from each other, making it difficult to compare them from the similar structural viewpoint. But, the more compact packing of stacked lamellae and the closer chain packing in the crystallites may give the stronger interactions between them, resulting in the mechanically tough microstructure. In this way, the present work has clarified for the first time an ideal microstructure giving an excellent mechanical properties, which can be obtained from an unexpectedly simple processing condition, *i.e.*, to increase the stretching rate and draw ratio in the BO process.

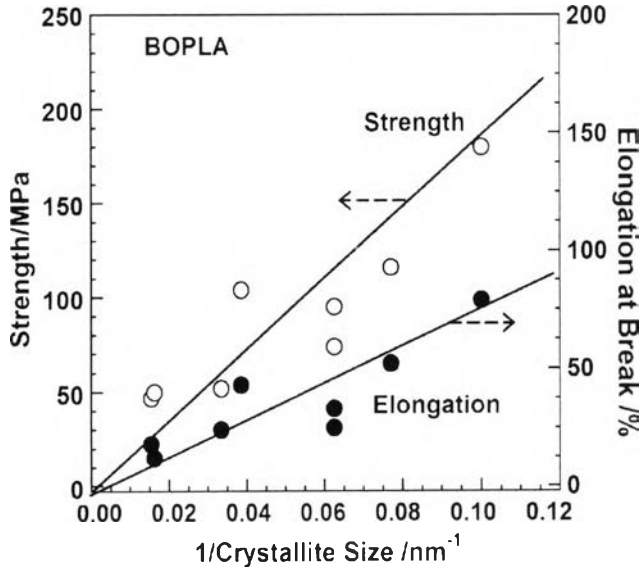

Figure 4.13 Relationship between the mechanical properties and the inversed crystallite size ((200/110) diffraction) plotted for a series of BOPLA films.

4.6 Acknowledgements

The authors wish to thank The Thailand Research Fund (the Royal Golden Jubilee Ph.D scholarship program PHD/0188/2550) for financial support as well as the Center for Petroleum, Petrochemical, and Advanced Materials, Chulalongkorn University for the research facilities. One of the authors (P. J.) would like to thank Dr. Taiyo Yoshioka for his assistance and suggestion.

4.7 References

[1] Auras R, Harte B, Selke S. Macromol Biosci 2004; 4: 835-64.

[2] Garlotta D. J Polym Environ 2002; 9: 63-84.

[3] Saeidlou S, Huneault MA, Li H, Park CB Prog Polym Sci 2012; 37: 1657-77.

[4] Chapleau N, Huneault MA, Li H. Int Polym Proc 2007; 5: 402-9.

[5] Martin O, Avérous L. Polymer 2001; 4: 6209-19.

[6] Li H, Huneault MA. Polymer 2007; 48: 6855-66.

[7] Xiao H, Lu W, Yeh JT. J Appl Polym Sci 2009; 113: 112-21.

[8] Kawamoto N, Sakai A, Horikoshi T, Urushihara T, Tobita E. J Appl Polym Sci 2007; 103: 198-203.

[9] Kulinski Z, Piorkowska E, Gadzinowska K, Stasiak M. Biomacromolecules 2006; 7: 2128-35.

[10] Zhang R, Wang Y, Wang K, Zheng G, Li Q, Shen C. Polym Bull 2012; 70: 195-206.

[11] Yu L, Liu H, Xie F, Chen L, Li X. Polym Eng Sci 2008; 48: 634-41.

[12] Ajji A, Dumoulin M. Biaxially oriented polypropylene (BOPP) processes. In *Polypropylene*; Karger-Kocsis, J., Ed.; Springer Netherlands; 1999.

[13] Breil J. Oriented film technology. In *Multilayer Flexible Packaging*; Wagner, J. R., Ed.; William Andrew Publishing: Boston; 2010.

[14] Jang J, Lee DK. Polymer 2004; 45: 1599-1607.

[15] Jiang M, Lin S, Jiang W, Pan N. Appl Surf Sci 2014; 311: 101-6.

[16] Briston JH, Katan LL. In Plastics films; 3rd ed.; Longman Scientific & Technical: England; 1989.

[17] Bobovitch AL, Tkach R, Ajji A, Elkoun S, Nir Y, Unigovski Y, Gutman EM. J Appl Polym Sci 2006; 100: 3545-53.

[18] Ania F, Calleja FJB, Bayer RK. Polymer 1992; 33: 233-8.

[19] Lüpke T, Dunger S, Sänze J, Radusch HJ. Polymer 2004; 45: 6861-72.

[20] Wang J, Zhu Y, Fu Y. Appl Surf Sci 2013; 285: 697-701.

[21] Lin YJ, Dias P, Chen HY, Hiltner A, Baer E. Polymer 2008; 49: 2578-86.

[22] Uejo H, Hoshino S. Appl Polym Sci 1970; 14: 317-28.

[23] Auras RA, Harte B, Selke S, Hernandez R. J Plast Film Sheet 2003; 19: 123-35.

[24] Lee MS, Paulino CM, Mizumura T, Chang K, Yokota N, Masuda J., US Patent 2010/0247886 A1; 2010.

[25] Cloutier JRC, Mizumura T, Chang KP. US Patent 20100040904; 2010.

[26] Dou S, Warwick RI, Lee MS, Chang KP. WIPO Patent WO/2010/148105 A1; 2010.

[27] Paulino CM, Yokota N. US Patent 20120141766; 2012.

[28] Sukigara MJ, Itada M, Koike H, Yatsuzuka M, Hamada Y. US Patent 20050008815; 2005.

[29] Ou X, Cakmak M. Polymer 2008; 49: 5344-52.

[30] Ou X, Cakmak M. Polymer 2010; 51: 783-92.

[31] Smith PB, Leugers A, Kang S, Hsu SL, and Yang X. J Appl Polym Sci 2001; 82:2497-2505.

[32] Tsai CC, Wu RJ, Cheng HY, Li SC, Siao YY, Kong DC, Jang GW. Polym Degrad Stabil 2010; 95: 1292-8.

[33] Delpouve N, Stoclet G, Saiter A, Dargent E, Marais S. J Phys Chem B 2012; 116: 4615-25.

[34] Fischer EW, Sterzel H, Wegner G. Kolloid Z. Z. Polym 1973; 251: 980-90.

[35] Patterson A. Physical Review 1939; 56: 978-82.

[36] Klug HP, Alexander LE. In X-ray Diffraction Procedures for Polycrystalline and Amorphous Materials; 2nd ed.; Wiley-Interscience: New York; 1974.

[37] Hoogsteen W, Postema AR, Pennings AJ, Ten Brinke G, Zugenmaier P. Macromolecules 1990; 23: 634-42.

[38] Kokturk G, Piskin E, Serhatkulu TF, Cakmak M. Polym. Eng. Sci. 2002; 42: 1619-28.

[39] Oh MO, Kim SH. Polym. Int. 2014; 63: 1247-53.

[40] Stoclet G, Seguela R, Lefebvre JM, Rochas C. Macromolecules 2010; 43: 7228-37.

[41] Stoclet G, Seguela R, Vanmansart C, Rochas C, Lefebvre JM. Polymer 2012; 53: 519-28.

[42] Wasanasuk K, Tashiro K. Macromolecules 2011; 44: 9650-60.

[43] Na B, Lv R, Zou S, Li Z, Tian N, Fu Q. Macromolecules 2010; 43: 1702-5.

[44] Delpouve N, Delbreilh L, Stoclet G, Saiter A, Dargent E. Macromolecules 2014; 47: 5186-97.

[45] Stoclet G, Seguela R, Lefebvre JM, Elkoun S, Vanmansart C. Macromolecules 2010; 43: 1488-98.

[46] Tsuji H, Ogiwara M, Saha SK, Sakaki T. Biomacromolecules 2006; 7: 380-87.

[47] Tsuji H, Ikada Y. Polymer 1995; 36: 2709-16.

[48] Rosenberg SJ, Gagon DH. J Res Nat Bur Stand 1941; 27: 159-69.